431 kA/cm^2 peak tunneling current density in GaN/AlN resonant tunneling diodes

Tyler A. Growden, Weidong Zhang, Elliott R. Brown, David F. Storm, Katurah Hansen, Parastou Fakhimi, David J. Meyer, and Paul R. Berger

Citation: Appl. Phys. Lett. **112**, 033508 (2018);

View online: https://doi.org/10.1063/1.5010794

View Table of Contents: http://aip.scitation.org/toc/apl/112/3

Published by the American Institute of Physics

431 kA/cm^2 peak tunneling current density in GaN/AlN resonant tunneling diodes

Tyler A. Growden,[1] Weidong Zhang,[2] Elliott R. Brown,[2] David F. Storm,[3] Katurah Hansen,[2] Parastou Fakhimi,[1] David J. Meyer,[3] and Paul R. Berger[1,a)]
[1]*Department of Electrical and Computer Engineering, The Ohio State University, Columbus, Ohio 43210, USA*
[2]*Departments of Physics and Electrical Engineering Wright State University, Dayton, Ohio 45435, USA*
[3]*U.S. Naval Research Laboratory, Washington, DC 20375, USA*

(Received 26 October 2017; accepted 2 January 2018; published online 19 January 2018)

We report on the design and fabrication of high current density GaN/AlN double barrier resonant tunneling diodes grown via plasma assisted molecular-beam epitaxy on bulk GaN substrates. A quantum-transport solver was used to model and optimize designs with high levels of doping and ultra-thin AlN barriers. The devices displayed repeatable room temperature negative differential resistance with peak-to-valley current ratios ranging from 1.20 to 1.60. A maximum peak tunneling current density (J_p) of 431 kA/cm^2 was observed. Cross-gap near-UV (370–385 nm) electroluminescence (EL) was observed above +6 V when holes, generated from a polarization induced Zener tunneling effect, recombine with electrons in the emitter region. Analysis of temperature dependent measurements, thermal resistance, and the measured EL spectra revealed the presence of severe self-heating effects. *Published by AIP Publishing*. https://doi.org/10.1063/1.5010794

Over roughly the past 15 years, there has been a great deal of theoretical and experimental work done on various III-nitride tunneling devices, trying to extend from lateral field effect transistors (FETs) using the polarization induced in-plane two-dimensional electron gas (2DEG) to a vertical topology that requires current transport orthogonal to the 2DEGs. These thin vertical devices place an extreme constraint on the quality of the epitaxial growth, which has led to a lack of reproducible results. Much of the earlier III-nitride resonant tunneling diode (RTD) work[1–13] suffered from issues with charge-trapping, hysteresis, sweep-to-sweep repeatability, poor substrate quality, or lack of room temperature operation. Recently, however, there have been reports of repeatable, room temperature negative differential resistance (NDR) through many sweeps,[14–16] which required high quality growth atop bulk GaN substrates, better design of the asymmetric double barrier RTD, and enhanced device processing. While repeatable, the reported NDR exhibited poor peak-to-valley current ratios (PVCRs) and low peak tunneling current densities. One application for RTDs is as compact low-power consuming oscillator sources,[17,18] but these oscillators require high current densities and large PVCRs to generate significant microwave power output. Previous researchers have reported very respectable current densities exceeding 100 kA/cm^2; however, the NDR was only observable at temperatures below 100 K and exhibited a modest PVCR of 1.03.[11]

In this letter, we investigate design methods, both theoretical and experimental, to improve both the PVCR and current density of state-of-the-art GaN/AlN RTDs. Data from our previously reported operational structure[15] were used to calibrate a quantum-transport simulation[15,19,20] which was then utilized for design optimization. From this, it was determined that the PVCR was most strongly affected by the ability to control the initial position, in energy, of the confined states within the quantum well (QW). This was accomplished by modifying the barriers, quantum well, and both unintentionally doped (UID) spacer thicknesses, as well as doping levels in both contact regions. Furthermore, during growth of the heavily doped bottom contact (emitter), it is possible that some of the silicon dopant could segregate to the growth surface and into the emitter spacer, which can lead to an increased valley current, I_v, as a result of enhanced impurity scattering. Subsequently, thick spacer layers were incorporated to reduce impurity accumulation within the active region. It is worth mentioning that while scattering from ionized impurities is a concern, piezoelectric acoustic phonon scattering is thought to be a much larger issue. Additionally, the well/barrier interface roughness has also been shown to be a significant scattering mechanism within these devices.[13]

It was determined that the best way to increase the peak tunneling current was to reduce the barrier thickness to 1.5 nm, while simultaneously decreasing the QW thickness to 2.5 nm. The QW thickness was decreased to maintain control over the positioning of the confined energy levels. This can be challenging in a GaN/AlN RTD as the energy band diagram becomes heavily distorted due to the presence of strong spontaneous and piezoelectric polarization effects at the heterointerfaces, which leads to a convoluted energy-band profile in the double-barrier structure, and large built-in electric fields. Each barrier can be thought of as having three distinct energy zones: triangular AlN at the highest energy, rectangular AlN in the middle, and a polarization induced AlN/GaN trapezoid at the bottom [Fig. 1(a)]. By controlling the initial energy levels for each state within the QW, the transmission probability through the double barrier system can be tailored for high current density. Ideally, at a certain bias voltage, the two-dimensional quasi-bound emitter state

a)Author to whom correspondence should be addressed: pberger@ieee.org. Also at: Department of Physics, The Ohio State University, Columbus, OH 43210-1106, USA.

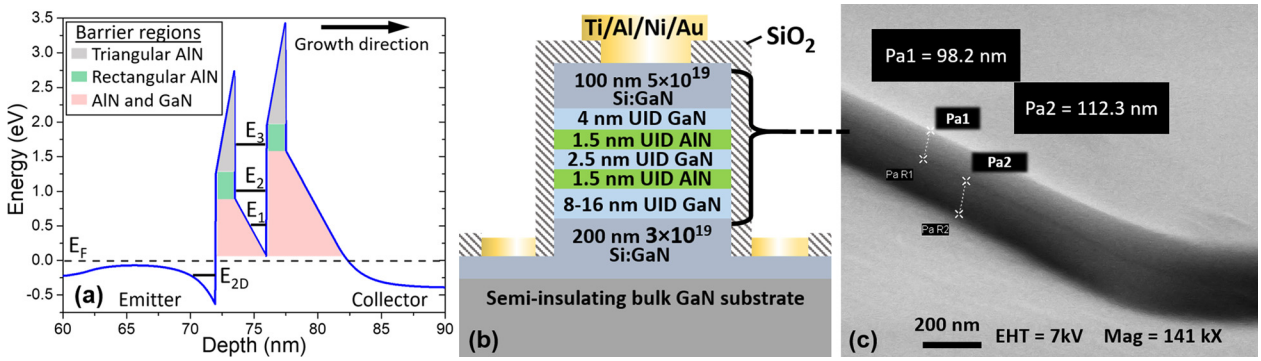

FIG. 1. (a) Simulated energy band diagram at 0 V bias, illustrating multiple barrier regions and confined energy levels. (b) Illustration of the device stack after fabrication. (c) Cross-sectional SEM image of the mesa sidewall prior to oxide deposition.

E_{2D}, in the region of electron accumulation just outside the barrier, aligns with the desired QW state (E_2 for these devices) at a level in the rectangular AlN barrier zones [green regions in Fig. 1(a)]. Unlike GaAs or InP-based RTDs, E_{2D} is located in a 2DEG which is polarization-induced and therefore not dependent upon applied voltage for its formation; furthermore, with the accumulation of well depths exceeding 0.6 eV at 0 V bias, stronger confinement can be achieved. While testing previous GaN/AlN RTDs of similar design, cross-gap (~360 nm) electroluminescence was observed due to the radiative recombination of electrons with holes. The holes are generated via Zener electron tunneling through the UID GaN collector spacer, starting from the emitter region. Greater details regarding this phenomenon were reported elsewhere.[21] Consequently, for the application of an RTD, this is another leakage source which increases I_v. To suppress this effect, the UID collector spacer was decreased to 4 nm.

The optimized design, displayed in Fig. 1(b), was grown by RF-plasma assisted molecular-beam epitaxy (MBE) on $18 \times 18\,mm^2$ freestanding semi-insulating Ga-polar GaN substrates. Details regarding sample preparation and growth parameters can be found elsewhere.[16,22,23] Device fabrication was performed using standard semiconductor mesa processing techniques; greater details can be found in our previous report.[15] Cross-sectional scanning electron microscope (SEM) imaging was used to verify the presence of vertical sidewalls, etch depth, mesa area (4.3 μm^2 and 11 μm^2), and top contact layer thickness [Fig. 1(c)]. It is worth noting that multiple samples with varying emitter spacer thicknesses (8, 12, and 16 nm) were grown sequentially during this study; however, no discernable differences in electrical behavior were observed during device characterization.

Figure 2(a) shows the current density vs voltage (J-V) characteristic of a typical 11 μm^2 device at room temperature before and after contact alloying via rapid thermal annealing (RTA). Because the top GaN contact layer is heavily doped, the as-deposited Ti/Al/Ni/Au contacts are Ohmic ($\sim 2 \times 10^{-5}$ $\Omega \cdot cm^2$). To avoid contact-spiking through the active region, a two-step RTA process with a maximum temperature of 720 °C was developed, resulting in a contact resistance of $\sim 1 \times 10^{-6}$ $\Omega \cdot cm^2$. The post-anneal J-V exhibited a 2.7 V decrease in the peak NDR voltage V_p as well as a PVCR increase resulting from a reduction in I_v. The post-anneal closed-loop voltage sweep began at −6 V, then up to +7.75 V, and finally back down to −6 V. This range was chosen because when the applied bias exceeded V_p by more than ~1.5–2.0 V, electric breakdown usually occurred. We have observed similar breakdown in previous sample designs, and they usually manifest as a short circuit followed almost immediately by contact failure, resulting in an open circuit. The mechanism by which the breakdown occurs is likely an interaction between the external-voltage bias field and the large internal GaN/AlN polarization discontinuities (~10 MV/cm).

Operational devices displayed repeatable and hysteresis free NDR, with PVCRs ranging from 1.2 to 1.6, and J_p values between 180 kA/cm^2 and 431 kA/cm^2. Figure 2(b) displays the increasing and decreasing I-V reproducibility under positive bias. The quantum-transport simulations indicate that the predominant peak is associated with resonant tunneling through the second quasibound level E_2 shown in Fig. 1(a). Additionally, the first derivative of the current with respect to the applied voltage reveals a feature at ~2.75 V, which is indicative of resonant tunneling through the first quasibound level E_1. This feature was observed in most of our devices and has been reported in GaN/AlN RTDs by others as well.[11,13,14] Repeatability was verified by conducting 500 individual voltage sweeps over the course of roughly two hours. The results shown in Fig. 2(c) display a high degree of repeatability; however, both the mean and standard deviation show a large variation within the "plateau" feature of the NDR region. This plateau is thought to be a time-averaged self-oscillation that becomes more pronounced at high current densities, which explains the observed deviation. Despite the high degree of variation within the plateau region, the peak current I_p was very stable with a coefficient of variation of 3×10^{-3}. The peak voltage between all devices was between +6.25 V and +7.10 V, which is a broader variation than in typical GaAs- or InP-based RTDs, but is likely a reflection of the nascent GaN technology and its lingering epitaxy and process variations. A couple of the smaller area devices, such as the one shown in Fig. 2(d), displayed anomalously large current densities up to 431 kA/cm^2, while maintaining high PVCRs (>1.3). This device was swept over 20 times and only exhibited a slight shift of V_p as the contacts "burned-in." The plateau displayed a very pronounced shelf with a positive slope and a slight hysteresis, which is not uncommon in this region. The peak current density of an RTD has an exponential dependence on the barrier

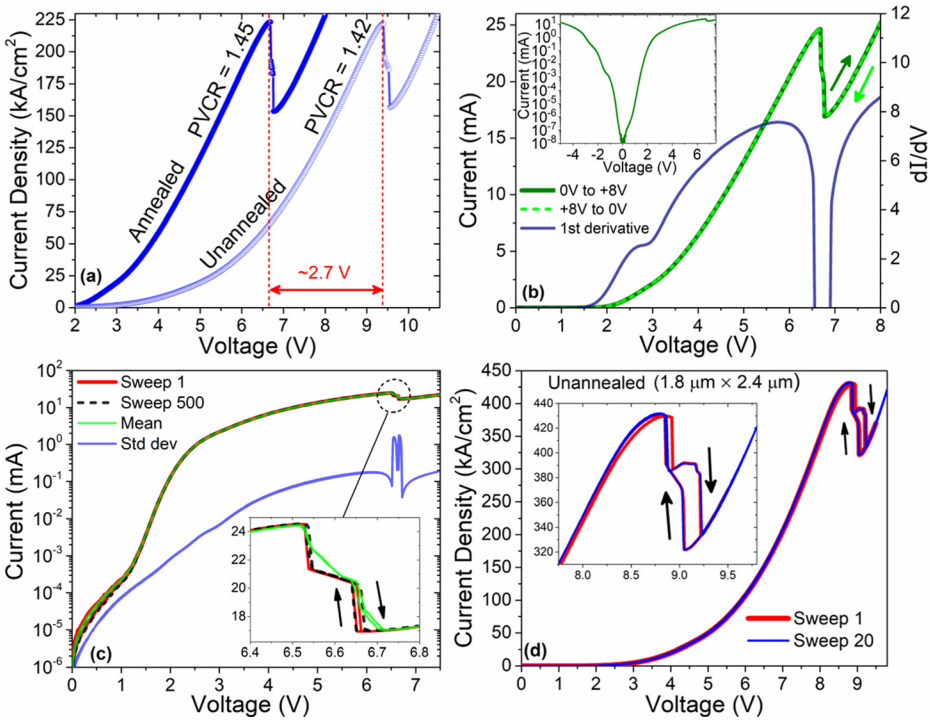

FIG. 2. (a) Current density vs voltage characteristics before and after contact RTA treatment. (b) Current vs voltage characteristic displaying forward sweep, reverse sweep, and derivative of current with respect to voltage. The inset displays a full semilog I-V swept from −5 V to +7.75 V and back. (c) Semilog plot displaying the I-V repeatability through 500 bidirectional sweeps. Inset displaying both sweep directions in the NDR region. (d) Bidirectional J-V curve displaying anomalous high current density from a small area device with slight hysteresis in the NDR region. Inset: magnified NDR region.

thickness; in fact, previously reported quantum-transport simulations[19] of similar GaN/AlN RTDs have shown that a two monolayer (∼0.5 nm) decrease in the AlN barrier thickness can result in a current increase of nearly 5000%. Considering this, it is very possible that the smaller devices were more susceptible to statistical (i.e., "monolayer") fluctuations in barrier thickness, as the observed current densities spanned a much larger range. However, the efficacy of the SiO_2 passivation layer has not yet been determined, so it is also possible that the increased current observed in the smaller devices is partially due to sidewall leakage.

Low temperature measurements were also carried out at 8, 50, 100, and 297 K [displayed in Fig. 3(a)]. It was observed that I_p remains stable; however, I_v begins to rise at temperatures above 100 K. This is a commonly observed effect in RTDs because the scattering effects, which contribute more strongly to I_v, are suppressed slightly at lower temperatures. Figure 3(b) displays high temperature I-V measurements, from a different device of the same design, and again, I_p remained stable, while I_v continued to increase. The heated probe station platen could not safely operate above 475 K, but if the I_v trend observed in Fig. 3(b) continues, then by extrapolation, the NDR would disappear above ≈485 K. This sets an upper limit on operational temperatures for these specific RTDs. Based on a theoretical model of $GaN/Al_xGa_{1-x}N$ heterostructures given by Ridley[24] and an approximation that the incoherent phonon-assisted valley tunneling current is proportional to the inverse of the scattering time constant, $1/\tau$, a simple analysis of I_v at both low and high temperatures (Fig. 3) shows that I_v can be written into a sum of two terms: one term tends to be a constant as the temperature approaches zero and the second term has a linear temperature dependence. The first term is attributable to LO phonon scattering via phonon emission, which has a very weak temperature dependence given by $1-\exp\left(-\frac{\hbar\omega_{LO}}{k_BT}\right)$. The exponential factor is $\ll 1$ because $\hbar\omega_{LO}$, the LO phonon energy, is ∼90 meV for GaN. Therefore, $\hbar\omega_{LO} \gg k_BT$ where k_B is the Boltzmann constant. The second term likely comes from piezoelectric acoustic phonon scattering, whose cross section has a linear dependence on temperature. A better understanding of the underlying physical mechanisms—primarily a mixing of LO phonon and piezoelectric acoustic phonon scattering—should help reduce the high valley current and thus improve the PVCR.

As the current density of a device increases, self-heating from I^2R resistive losses in the mesa structure becomes

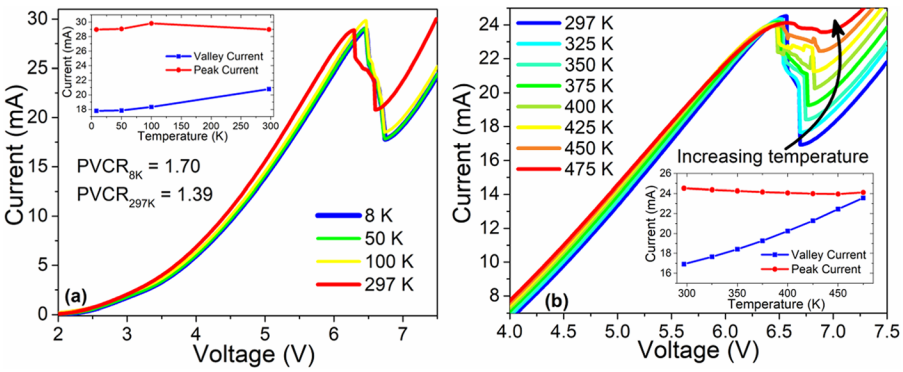

FIG. 3. (a) Low temperature I-V sweeps illustrating a significant change in valley current. (b) High temperature I-V sweeps showing the disappearance of NDR as temperature increases. Insets: peak and valley current values displaying the temperature dependence of differing current mechanisms.

prevalent, especially within the lower doped regions and, depending on their quality, the Ohmic contacts as well. If the heating effects are severe enough, the device performance will begin to suffer, much like what is observed in Fig. 3(b). The RTDs reported here were grown atop bulk GaN substrates, which provide much greater thermal conductance for a given surface-fabricated device than their sapphire-substrate counterparts. However, the current densities reported here are still sufficiently high to cause device performance degradation in the mesa geometry. An approximation of self-heating was calculated [Figs. 4(a) and 4(b)] using the method outlined by Brown,[25] which assumes that the device dimensions are much smaller than the substrate. Therefore, the device is treated as a small disk of heat on a thermally conducting half-space. The change in temperature from Joule heating can then be calculated using $\Delta T = I{\cdot}V[\sqrt{2}\kappa\pi r]^{-1}$, where V is the applied bias, I is the average current, κ is the thermal conductivity [$\sim$1.3 W/cm K for GaN], and r is the equivalent device radius [cm]. The heat transfer curves in Fig. 4(a) were calculated assuming thermal resistances of 1480 and 925 °C/W for the 4.3 and 11.0 μm^2 devices, respectively. These are determined primarily by downward vertical heat conduction in the GaN/AlN mesa and then spreading from the bottom of the mesa into the GaN epitaxial layer and substrate below. The top-side metal contact also conducts some heat away from the active device region laterally through a wedge made of the same metallization as the top contact. The wedge taper starts with a width of the device under test and ends in a width of 40 μm, over a distance of 67 μm, where it becomes the center conductor of the GSG line. Because of the small cross section of the wedge at the device end, and its length, the thermal resistance is very high compared to the vertical conduction value. Using a numerical integration technique, values of 5.6×10^4 and 5.1×10^4 °C/W were calculated for the 4.3 and 11.0 μm^2 devices, respectively, making them negligible compared to the vertical thermal resistances.

Despite the added leakage current due to Zener tunneling through the collector spacer, the subsequent hole generation results in cross-gap light emission—a useful aid in device characterization. Because the method utilized for determining ΔT from thermal resistance was based on multiple assumptions, we can test its accuracy by analyzing the electroluminescence (EL) spectra. Displayed in Figs. 4(c) and 4(d) are the spectra for the same two devices used for Figs. 4(a) and 4(b), as the current is increased. There is a pronounced red shift in the peak energy as the current is increased, which is further evidence of the self-heating effects. Because the light emission is cross-gap, a comparison of the well-known Varshni bandgap formula

$$E_g(T) = E_g(0) - \frac{\alpha T^2}{T + \beta} \tag{1}$$

can be made with the measured peak emission energy and the calculated ΔT at each current value. The values used for the Varshni coefficients, as reported by Vurgaftman *et al.*,[26] were $\alpha = 0.909$ meV/K and $\beta = 830$ K. However, an accurate representation of the bandgap for such a heavily doped sample requires the additional consideration of bandgap renormalization (BGR) and the Burstein-Moss (BM) effect. BGR is an effect which causes the bandgap to decrease with the increasing carrier concentration.[27] Conversely, the BM effect causes an increase in the effective bandgap as the carrier concentration increases.[28,29] Bouzidi *et al.* conducted a study of these competing effects, as well as strain-induced effects, in heavily doped GaN and found a strong dependence of the effective bandgap on the Si doping concentration.[30] In our previous report on a similar device, we found that the light emission was taking place in the emitter region which, in this case, is doped 3×10^{19} cm^{-3} GaN:Si. Using the corrected values from Bouzidi for $E_{g\_300\,K}$, $E_g(0)$ was calculated and then $E_g(T)$ was plotted from 300 K up to 800 K [Fig. 4(e)]. By then combining the values for ΔT [Figs. 4(a) and 4(b)] and the peak emission energies [Figs. 4(c) and 4(d)] for a given bias, a comparison was made to the corrected bandgap [illustrated in Fig. 4(e)] and found to be in very close agreement. Thus, it can be observed that when biased around the NDR region and beyond, the internal GaN/AlN RTD device temperatures are estimated to increase by roughly 190–300 °C.

In summary, we have reported experimental data and theoretical considerations for high current density GaN/AlN RTDs. Designs were optimized with the aid of quantum-transport simulations and previous experimental results. By decreasing the AlN barrier thicknesses to 1.5 nm, while still maintaining control of the QW bound states, current densities reaching 431 kA/cm^2 were achieved, while also maintaining highly repeatable NDR with respectable PVCRs. A

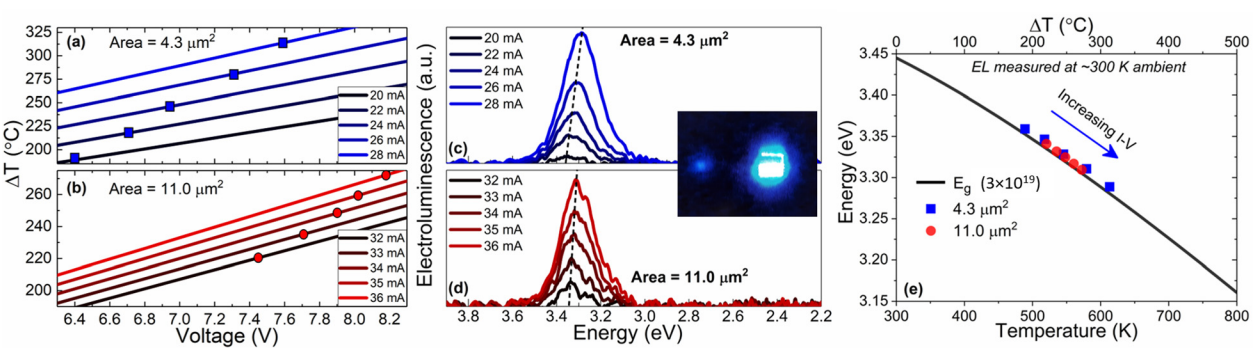

FIG. 4. Change in temperature resulting from thermal resistance in devices with areas of (a) 4.3 μm^2 and (b) 11.0 μm^2. The symbolized points are where the EL measurements in (c) and (d) were taken. EL intensity vs emission energy at multiple current levels for devices with areas of (c) 4.3 μm^2 and (d) 11.0 μm^2. Inset: optical image of the 11.0 μm^2 RTD light emission. (e) Bandgap vs temperature calculated with Eq. (1). Also displayed are the self-heating effects from (a) and (b) combined with the peak emission energy from (c) and (d).

high degree of repeatability was observed across 500 I-V sweeps, and further, the standard deviation displayed a large variation in the plateau of the NDR region consistent with oscillatory behavior. Temperature dependent measurements were carried out on multiple devices from 4 K up to 475 K. The peak current remained stable throughout the entire range; however, the valley current continued to increase until the NDR disappeared at ≈485 K. This was analyzed in the context of likely phonon scattering mechanisms. In addition, electroluminescence spectra and thermal resistance calculations were used to analyze the self-heating effect in these devices. The red-shifted luminescence spectra and the ΔT value from self-heating effects displayed a strong correlation with the expected bandgap temperature dependence $E_g(T)$, suggesting that this device analysis approach is valid. This will allow for greater insight into how physical parameters affect future device designs as high-current-density GaN/AlN RTDs advance to electronic and photonic applications.

The authors would like to acknowledge funding from Office of Naval Research under the "DATE" MURI program (N00014-11-1-0721, program manager: Dr. Paul Maki).

[1]A. Kikuchi, R. Bannai, K. Kishino, C. M. Lee, and J. I. Chyi, Appl. Phys. Lett. **81**, 1729 (2002).
[2]K. Kishino and A. Kikuchi, Phys. Status Solidi A **190**, 23 (2002).
[3]S. N. Grinyaev and A. N. Razzhuvalov, Semiconductors **37**, 433 (2003).
[4]C. T. Foxon, S. V. Novikov, A. E. Belyaev, L. X. Zhao, O. Makarovsky, D. J. Walker, L. Eaves, R. I. Dykeman, S. V. Danylyuk, S. A. Vitusevich, M. J. Kappers, J. S. Barnard, and C. J. Humphreys, Phys. Status Solidi C **7**, 2389 (2003).
[5]M. Hermann, E. Monroy, A. Helman, B. Baur, M. Albrecht, B. Daudin, O. Ambacher, M. Stutzmann, and M. Eickhoff, Phys. Status Solidi C **8**, 2210 (2004).
[6]S. Golka, C. Pflugl, W. Schrenk, and G. Strasser, Appl. Phys. Lett. **88**, 172106 (2006).
[7]C. Bayram, Z. Vashaei, and M. Razeghi, Appl. Phys. Lett. **96**, 042103 (2010).
[8]Z. Vashaei, C. Bayram, and M. Razeghi, J. Appl. Phys. **107**, 083505 (2010).
[9]L. Yang, H. He, W. Mao, and Y. Hao, Appl. Phys. Lett. **99**, 153501 (2011).
[10]T. A. Growden, S. Krishnamoorthy, D. N. Nath, A. Ramesh, S. Rajan, and P. R. Berger, in *IEEE Device Research Conference* (University Park, PA, 18–20 June 2012), pp. 163–164.
[11]D. Li, L. Tang, C. Edmunds, J. Shao, G. Gardner, M. J. Manfra, and O. Malis, Appl. Phys. Lett **100**, 252105 (2012).
[12]D. Li, J. Shao, L. Tang, C. Edmunds, G. Gardner, M. J. Manfra, and O. Malis, Semicond. Sci. Technol. **28**, 074024 (2013).
[13]A. Grier, A. Valavanis, C. Edmunds, J. Shao, J. D. Cooper, G. Gardner, M. J. Manfra, O. Malis, D. Indjin, Z. Ikonic, and P. Harrison, J. Appl. Phys. **118**, 224308 (2015).
[14]J. Encomendero, F. A. Faria, S. M. Islam, V. Protasenko, S. Rouvimov, B. Sensale-Rodriguez, P. Fay, D. Jena, and H. G. Xing, Phys. Rev. X **7**, 041017 (2017).
[15]T. A. Growden, D. F. Storm, W. Zhang, E. R. Brown, D. J. Meyer, P. Fakhimi, and P. R. Berger, Appl. Phys. Lett. **109**, 083504 (2016).
[16]D. F. Storm, T. A. Growden, W. Zhang, E. R. Brown, N. Nepal, D. S. Katzer, M. T. Hardy, P. R. Berger, and D. J. Meyer, J. of Vac. Sci. & Tech. B, Nanotechnol. and Microelectron.: Mater, Process., Meas., and Phenom. **35**(2), 02B110 (2017).
[17]E. R. Brown, J. R. Söderström, C. D. Parker, L. J. Mahoney, K. M. Molvar, and T. C. McGill, Appl. Phys. Lett. **58**, 2291 (1991).
[18]M. Feiginov, C. Sydlo, O. Cojocari, and P. Meissner, Appl. Phys. Lett. **99**, 233506 (2011).
[19]T. A. Growden, Ph.D. thesis, The Ohio State University, Columbus, 2016.
[20]See www.silvaco.com for Silvaco ATLAS [software], 2016.
[21]T. A. Growden, W. Zhang, Elliott R. Brown, D. F. Storm, D. J. Meyer, and P. R. Berger, "Near-UV electroluminescence in unipolar-doped, bipolar-tunneling (UDBT) GaN/AlN heterostructures," Light: Science & Applications (to be published).
[22]D. F. Storm, D. A. Deen, D. S. Katzer, D. J. Meyer, S. C. Binari, T. Gougousi, T. Paskova, E. A. Preble, K. R. Evans, and D. J. Smith, J. Cryst. Growth **380**, 14 (2013).
[23]D. F. Storm, T. O. McConkie, M. T. Hardy, D. S. Katzer, N. Nepal, D. J. Meyer, and D. J. Smith, J. Vac. Sci. Technol., B: Nanotechnol. Microelectron.: Mater., Process., Meas., Phenom. **35**(2), 02B109 (2017).
[24]B. K. Ridley, B. E. Foutz, and L. F. Eastman, Phys. Rev. B **61**, 16862 (2000).
[25]E. R. Brown, "Terahertz generation by photomixing in ultrafast photoconductors," in *Terahertz Sensing Technology*, edited by D. L. Woolard, W. R. Loerop, and M. S. Shur (World Scientific, Singapore, 2003), pp. 147–195.
[26]I. Vurgaftman and J. R. Meyer, J. Appl. Phys. **94**, 3675 (2003).
[27]K. F. Berggren and B. E. Sernelius, Phys. Rev. B **24**, 3240 (1981).
[28]E. Burstein, Phys. Rev. **93**, 632 (1954).
[29]T. S. Moss, Proc. Phys. Soc. B **67**, 775 (1954).
[30]M. Bouzidi, Z. Benzarti, I. Halidou, S. Soltani, Z. Chine, and B. El Jani, Mater. Sci. Semicond. Process. **42**, 273 (2016).